Original Research Article

Effects of extraosseous talotarsal stabilization on the biomechanics of flexible flatfoot subtalar joints in children: a finite element study

Xiangyu Cheng[1], Zhiqin Deng[1], Weidong Song[2], Jianquan Liu[1], Wencui Li[1]*

[1]Department of Hand and Foot Surgery, Shenzhen Second People's Hospital, Shenzhen University, Shenzhen, China
[2]Department of Orthopedics, Sun Yat-sen Memorial Hospital, Sun Yat-sen University, Guangzhou, China

*Correspondence:
Dr. Wencui Li,
E-mail: liwencui@email.szu.edu.cn

ABSTRACT

Background: Objective of the study was to generate an experimental foundation for the clinical application of extraosseous talotarsal stabilization (EOTTS) in treatment of flexible flatfeet in children by investigating the biomechanical characteristics of flexible flatfoot and the effects of EOTTS on hindfoot biomechanics.
Methods: Three-dimensional finite element models of the foot and ankle complex were generated from computer tomography images of a volunteer's left foot in three states: normal, flexible flatfoot, and post-EOTTS. After validation by X-ray, simulated loads were applied to the three models in a neutral position with both feet standing.
Results: In the flexible flatfoot model, the contact stress on the subtalar joint increased and contact areas decreased, resulting in abnormal stress distribution compared to the normal model. However, following treatment of the foot with EOTTS, these parameters returned to close to normal. Subtalar joint instability leads to a flexible flat foot. Based on this study, it is proposed that EOTTS can restore the normal function of the subtalar joint in and is an effective treatment for flexible flatfoot in children. We and many clinical data studies provide evidence for sinus tarsi implants in pediatric patients. It is showed that the formation of flexible flatfoot is induced by subtalar joint instability.
Conclusions: Because of the EOTTS provides the best biomechanical solution to subtalar joint instability, the EOTTS became an effective form for subtalar joint instability treatment.

Keywords: Subtalar joint, Flatfoot, Finite element analysis, Biomechanical phenomena, Extraosseous talotarsal stabilization, Sinus tarsi stent/implant

INTRODUCTION

A flatfoot is the result of a combination of deformities. Specifically, the primary deformity is the talar instability. Study has been demonstrated that medial displacement calcaneal osteotomy has little to no impact on talar realignment.[1] Other studies show that the deformity of calcaneus being in the valgus position, which also results in the talus having a medial plantar tilt that leads to a reduction in or absence of the longitudinal arch.[2] Flatfoot can be categorized as being either flexible or rigid and the method of treatment depends on this designation. When non-weight-bearing, a flexible flatfoot has a normal architecture and excessive midtarsal and talotarsal joint pronation with clear collapse of the medial arch during both static and dynamic weight-bearing.[3,4] While the majority of cases of flexible flatfoot in children remain asymptomatic, those cases that are symptomatic need to be treated with either conservative or surgical approaches.[5,6]

There is no overall consensus on the optimal method of treatment. However, there is a consensus on a stable hindfoot being critical to foot, ankle, and proximal musculoskeletal chain biomechanics.[7,8] Since the recovery for osseous reconstructive surgeries is prolonged, subtalar

arthroereisis is recommended due to the subtalar joint alignment being restored. It is suggested an implant be positioned in the tarsal sinus, but there is no consensus on issues related to biomechanical changes in the hindfoot and proximal musculoskeletal structures.

Extraosseous talotarsal stabilization (EOTTS) is a special type of talotarsal arthroereisis. A representative extraosseous talotarsal stabilizer, HyProCure has been the most widely used device for EOTTS. Graham et al consider EOTTS to be applicable in flexible flatfoot with talotarsal partial dislocation with rigid flatfoot being a contraindication for EOTTS.[9] EOTTS is preferred for flexible flatfoot because it stabilizes the axis of the subtalar joint motion and, thus, restores the normal biomechanics of the hindfoot and allows patients to quickly perform weight-bearing activities. Recently, there has been a gradual rise in the use of EOTTS with HyProCure to treat flexible flatfoot in children in the clinic because the method is convenient, minimally invasive, and results in a good prognosis with fewer complications.[10]

After flexible flatfoot has been treated by EOTTS, an improvement in deformity, pain, instability, and other symptoms in children is often observed.[11] This raises the question of how HyProCure implantation causes biomechanical changes of the subtalar joint and whether EOTTS can restore the stability of the subtalar joint. At present, studies on the curative effect of EOTTS have been mostly clinical evaluations and have not been verified by fundamental experimental studies.[10,12,13] Currently, there is no robust biomechanical evidence available to support EOTTS as an optimal approach for distributing subtalar joint stress. Traditional research methods have failed to characterize the mechanism underlying force transmission in the interior of the subtalar joint. For example, cadaveric specimens often display notable individual differences and do not have physiologic function.[14]

Finite element (FE) analysis has been widely used in the field of medical science.[15,16] In particular, the three-dimensional (3D) FE method enables sensitive, effective, and reproducible mechanical analysis and can be used to characterize contact stress and evaluate facet stress distribution.[9]

The present study aimed to assess the influence of EOTTS using HyProCure stent positioned in the tarsal sinus on interior stress distribution in the subtalar joint. An understanding of the stress distribution within the subtalar joint could aid in better understanding the biomechanical behavior of the hindfoot.

METHODS

Data collection

This study was approved by the institutional review board of Sun Yat-sen Memorial Hospital. This is a pre-clinical study that collected 1 volunteer who was treated at Sun

Yat-sen Memorial Hospital in 2015. This volunteer was 12 years old, was 152 cm tall, and had a body mass of 40 kg. She did not have any bone, ligament, cartilage, vascular, or nerve injuries or infection of foot joints based on physical and radiological examinations.

She also had no foot deformity, abnormal gait, foot injury, tumors, or surgical history. Examination of the left foot revealed no pathologic features and, thus, was evaluated using radiographs and magnetic resonance imaging. Cross-sectional computed tomography (CT) images were obtained at 0.6 mm intervals in a plane 20 cm above the ankle traveling down to the sole of the foot.

A geometrically accurate FE model was generated by performing a 3D reconstruction of the obtained CT images of a female volunteer's left foot and ankle in a neutral unloaded position. This volunteer had not experienced previous trauma and had no other abnormalities when examined by radiograph. Next, 64-slice spiral CT scans were obtained as described above. The data were saved in digital imaging and communications in medicine (DICOM) format. Prior to evaluation by radiography and CT scan, the volunteer provided informed consent.

Numerical approach

The original DICOM format images were obtained by scanning the child's left foot using a 64-slice spiral CT, imported into Mimics software, and manually segmented to extract the target tissue. From this, a 3D geometric model of the subtalar joint was generated through the threshold segmentation and corresponding deletions performed according to the different gray values. Every bone was fit with highly accurate boundary surfaces using several techniques, both manual and automated, available in Mimics (Materialise, Leuven, Belgium). The 3D structures of the subtalar joint talus, calcaneus, and navicular were reconstructed using thresholding segmentation and region-growing tools.

Subsequently, the resulting data were exported in the point cloud file format and transferred into SolidWorks 2009 (SolidWorks Corporation, Concord, MA, USA). Geometric models were then created and the talotarsal complex, including the tibia, talus, fibula, calcaneus, and navicular, was constructed. The threshold operation was used to distinguish between bones and soft tissues, the resulting bone information was extracted, and a geometric 3D foot model was created from this extracted bone information and output as STL files.

FE models of a normal foot, flexible flatfoot, and post-EOTTS foot

The geometric model was exported as an STL file and then imported into the reverse-engineering software Geomagic studio to smooth the fitting surface, eliminate noise from the model, and process point cloud information. The resulting files were output as an IGES file from which an

entity suture model was generated using UG software by curve reconstruction with rapid form. To create an FE model of the entire foot, the resulting data were imported into the Simulation module, which allowed for 3D contacts, springs, torques, and forces to be applied. In addition, the IGES entity model was imported into the FE software Abaqus (version 12.0, professional version; Simulia, Providence, RI), as well as HyperWorks FE analysis processing software, where grid division was performed and material parameters and specific load set up. From this, a 3D FE model of a child's normal foot containing the talus, calcaneus, navicular bone, ligaments, tendons, and articular cartilage was output. There is a complete set of model adjustment and optimization procedures, mainly based on the position and angle of the X-ray bone, as shown in Figure 1. Based on the normal foot FE model, adjustments were made to the talus to adduction, the calcaneus to abduction, and the forefoot to pronation, while the fibula and tibia were fixed. The angles of adjustment were determined according to the X-ray images of the flexible flatfoot before surgery. A complete model of flexible flatfoot was created by assembling according to the original anatomic relationship.

An implant geometric model was established in Abaqus (Simulia) using the HyProCure parameter for clinical insertion in the tarsal sinus. According to the angles of the flexible flatfoot determined by X-ray images obtained after surgery, the HyProCure device and subtalar joint were assembled to adjust the model. In the 3D FE model, the stent insertion was performed under the following basic conditions. For this device type, the medially threaded cylindrical portion was positioned within the canalis of the tarsal sinus. The HyProCure device had a final position within the central half of the tarsal sinus, i.e. the center of this device (point of transition from the cylindrical to the conical aspect) ran along the longitudinal talar bisection line. Furthermore, the device was oriented along the natural alignment of the tarsal sinus, i.e. in an anterior-lateral-distal to posterior-medial-proximal manner. The geometric model of the complex was then imported into HyperWorks FE analysis processing software and a grid generated and assigned before processing, which lead to the output of a post-EOTTS 3D FE model. In this model, both the bone and stent were considered linear elastic materials.

Material parameters

In the simulation module, a new static example was generated based on the assembly. The parameters were selected according to the cortical and trabecular elasticity. Bony structures and stent were simulated for the isotropic linear elastic material, where the material properties of the bone and stent were determined based on the literature.[17] Specifically, the bone elastic modulus was considered 73 MPa, the Poisson ratio 0.3, the stent of the elastic modulus 200000 MPa, and Poisson's ratio 0.3. The bony structures were idealized as isotropic, homogeneous, and linearly elastic. The stent and talar contact friction coefficient was 0.4, the calcaneus and stent contact friction coefficient was 0.4, and the friction coefficient was 0.01 to establish contact with the articular surface. The structure of the bone and cartilage was modeled as an isotropic linear elastic material using nonlinear uniaxial ligament as a connecting unit to simulate the properties of tension and no compression. Bone, articular cartilage, ligament, and HyProCure were regarded as continuous, homogeneous, and isotropic linear elastic materials. The material attributes in these models are listed in Table 1. All the models in the neutral position were loaded by longitudinal forces to simulate body weight using the method of static loading. All the models were validated by X-ray.

Boundary and loading conditions

Loadings at neutral position of a single foot standing were simulated in all models. Here, the central points of the upper tibia and fibula were fixed with the remaining bones left free to move. To simulate standing and balancing on one foot while bearing a body mass of 40 kg, a vertical force of 400 N was applied to the upper tibia.

Observed indicators

We observed the stress distribution, stress concentration area, joint contact area, contact stress, and Von-Mises stress of the anterior, middle, and posterior articular surfaces of the subtalar joint and the talonavicular articular surfaces in the static state of weight-bearing. After all the experimental results were exported, the biomechanical changes in the three models were compared.

Table 1: Material attributes in the models.

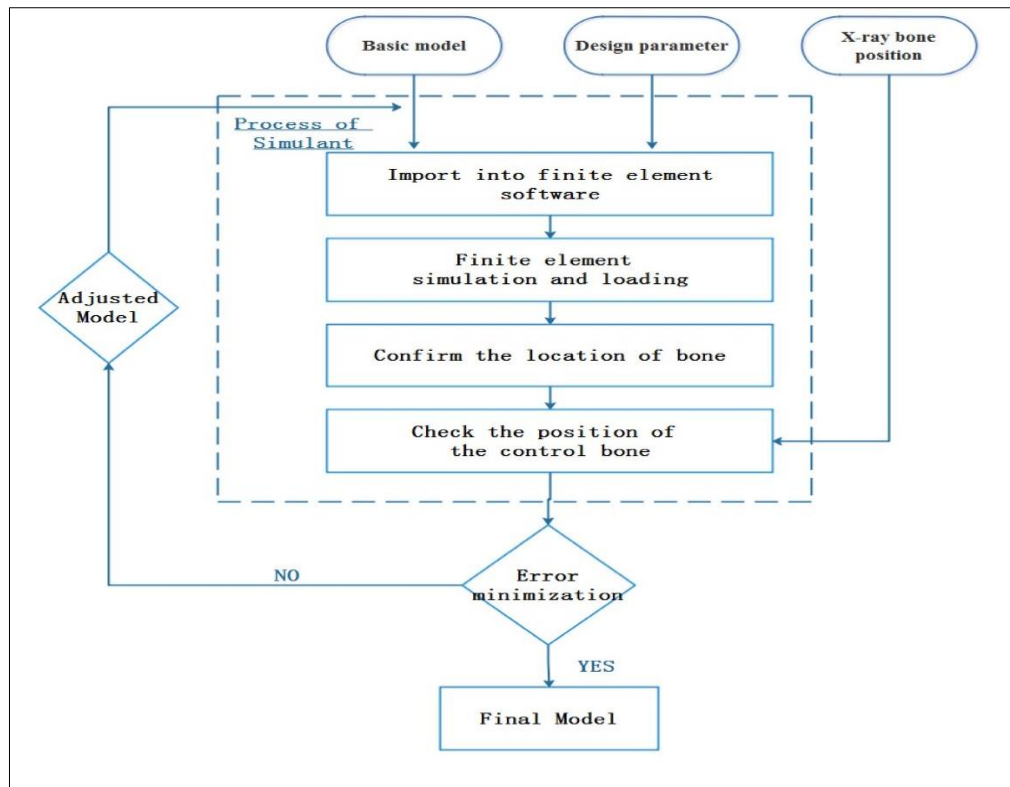| Materials	Elastic modulus (MPa)	Poisson's ratio	Bulk modulus (MPa)	Shear modulus (MPa)
Bone	7300	0.3	6083.3	2807.7
Cartilage	1	0.4	1.6667	0.35714
Ligament	260	0.4	433.33	92.857
HyProCure	103400	0.35	114890	38296
Sole	0.15	0.45	0.5	0.05172
Floor	17000	0.1	7083.3	7727.3

Continued.

Figure 1: Model adjustment and optimization procedures. Based on the basic foot model and design parameter, data will import into finite element software. Then finite element will simulate and load. The angles of adjustment were determined according to the X-ray images of the flexible flatfoot before surgery. A complete model of flexible flatfoot was output.

RESULTS

Establishment of models

Based on 3D CT scan data of a normal child's foot, we established the 3D FE model. Based on this model, we made adjustments according to the flatfoot and then simulated HyProCure implanting, thus establishing a 3D FE model of a post-EOTTS foot. A 3D FE model of a normal foot in children, including the bone, articular cartilage, main ligaments, and sole was generated with 1568634 nodes, 861755 units, and good geometric similarity (Figure 2a and b).

The FE model of the flexible flatfoot was based on the FE model of the normal foot, where the talus was adjusted to adduction, calcaneus to abduction, and forefoot to pronation and the fibula and tibia immobilized. This model contained 1611755 nodes and 883124 units (Figure 2c and d). The post-EOTTS foot model was established using Abaqus (Simulia) and HyProCure parameters for clinical insertion into the tarsal sinus. According to the angles of the flexible flatfoot in the X-ray images taken after surgery, the HyProCure device was assembled and the subtalar joint adjusted in the model. The resulting post-EOTTS foot model included 1684487 nodes and 916316 units (Figure 2e and f).

Validation of models

The models were validated based on plantar contact area, plantar stress distribution, peak stress, and bone positions in radiographs of the volunteer's foot. The normal foot, flexible flatfoot, and post-EOTTS foot models were similar to the entities and those previously described in the literature.[18-21] After applying boundary conditions and loads, the model's stress-strain results were compared with the results in the literature to verify the model's validity.[18-21] The experimental results are similar to those in most studies (including cadaver model, in-body study and finite element model), indicating that this experimental model is relatively reliable.

Biomechanical analysis/effects of EOTTS

All three models were imported into the FE analysis software, where load was applied in the neutral position to simulate the loading state of the human body and stress analysis of the subtalar joint was conducted. The stress distribution, stress increasing zone, joint contact area, contact stress, and von-Mises stress in the flexible flatfoot model in a weight-bearing stance were significantly different from in the model of the normal foot. The experimental results for the post-EOTTS model were similar to that of the model of a normal foot. The biomechanical values from the models of the flexible

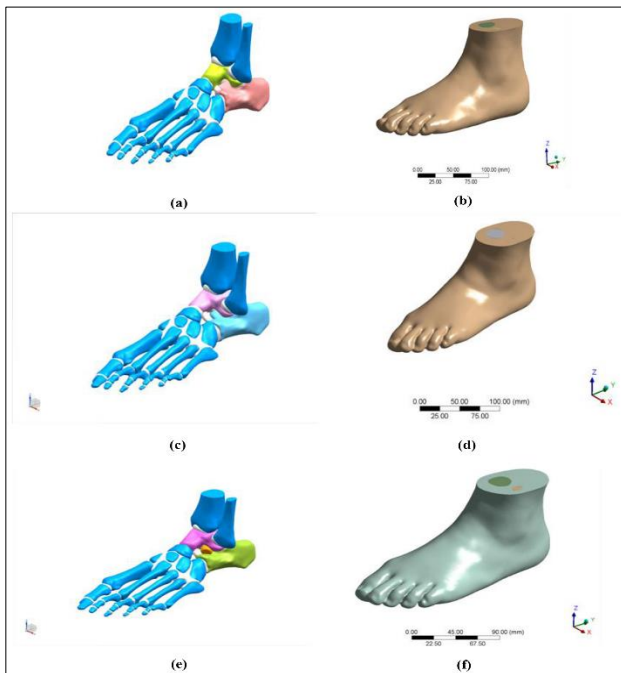flatfoot, post-EOTTS foot, and intact subtalar joint were compared.

Figure 2: Constructed normal, flexible and post-EOTTS foot of 3D FE models (a) entity model of preprocessing generates, (b) complete foot construction (including bone and soft tissue), (c) entity model of preprocessing generates, (d) output 3D finite element flexible foot model, (e) the entity post-EOTTS foot model of preprocessing generates, (f) output 3D finite element post-EOTTS foot model.

The maximum principal stress at each joint surface, which reflects the size and direction of contact stress, is shown in Table 2. The stress distribution diagram of the model is shown in the Figure 3. The maximum principal stress increased from the normal foot to the flatfoot and then decreased after EOTTS treatment of the subtalar and talonavicular joints. The maximum principal stress and local contact stress on the subtalar and talonavicular joints were too high in the flatfoot model. Compared to the normal foot model, the maximum principal stress on the subtalar and talonavicular joints tended to be concentrated during weight status, the main stress area was transferred, and the distribution of the contact stress was abnormal in the flatfoot model. However, the maximum principal stress concentration was diminished and the stress distribution normal in the post- EOTTS foot model.

As shown in Table 3 and Figure 4, von-Mises equivalent stress was analyzed. The contact stress of the joint is complex and, therefore, the maximum principal stress and von-Mises equivalent stress should be comprehensively investigated. Compared to the normal foot model, the von-Mises equivalent stress on the subtalar and talonavicular joints were overloaded in the flatfoot model. However, the von-Mises equivalent stress was close to normal in the post-EOTTS foot model. Compared to the normal foot model, the von-Mises equivalent stress on the subtalar and talonavicular joints tended to be concentrated in the flatfoot model during weight conditions. The distribution of the contact stress was abnormal. However, the von-Mises equivalent stress concentration was diminished and the stress distribution was close to normal in the post-EOTTS foot model. These trends displayed by the von-Mises equivalent stress were similar to those displayed by the maximum principal stress. Both of these types of stress reflect changing trends in contact stress distribution.

The contact areas of the articular surfaces in the talus and calcaneus are described in Table 4. Compared to the normal foot model, the contact areas of the articular surfaces of the subtalar and talonavicular joints were smaller in the flatfoot model and recovered to normal levels in the EOTTS simulation model. The decreases in the subtalar and talonavicular joint articular surface contact areas in the flatfoot model are mainly reflective of the mid-astragalus and rear-astragalus talonavicular articular. These recovered to normal in the post-EOTTS foot.

As shown in Table 5, the bone coordinates were analyzed. The variation tendency of each bone on the x-, y-, and z-axes differed between models. In the flat-footed model, the coordinates of astragalus on the x- and z-axes and calcaneus on the z-axis decreased. The coordinates of the calcaneus on the x-axis, navicular on the x- and z-axes, and cuboid on the x- and z-axes increased. However, there were no significant differences in the sitting values of the talus, calcaneal, navicular, and cuboid on the y-axis. This indicates the talus shows inward and downward displacement, calcaneal shows outward and downward displacement, and cuboid shows outwards and upwards displacement. The variation tendency of each bone on the x-, y-, and z-axes recovered to normal in the post-EOTTS model.

Table 2: Maximum principal stress of articular surface (MPa).

Paramet-ers	Astragalus joint surface				Calcaneal joint surface			
	Anterior-astragalus	Mid-astragalus	Rear-astragalus	Talona-vicular	Anterior-calcaneal	Mid-calcaneal	Rear-calcaneal	Calcane-ocuboid
Normal	0.39	0.79	1.13	0.39	0.35	0.22	0.53	1.37
Flatfoot	0.22	0.99	1.45	0.64	0.31	0.6	0.74	0.87
EOTTS	0.31	0.78	1.2	0.41	0.38	0.32	0.51	1.49

Table 3: Von-Mises stress of articular surfaces (MPa).

Paramet-ers	Astragalus joint surface				Calcaneal joint surface			
	Anterior-astragalus	Mid-astragalus	Rear-astragalus	Talona-vicular	Anterior-calcaneal	Mid-calcaneal	Rear-calcaneal	Calcane-ocuboid
Normal	0.57	0.86	1.29	0.61	0.57	0.21	0.6	1.91
Flatfoot	0.48	1.29	1.65	0.85	0.51	1.57	1.22	1.24
EOTTS	0.56	1	1.34	0.65	0.53	0.45	0.8	1.99

Table 4: Contact area of articular surface (mm^2).

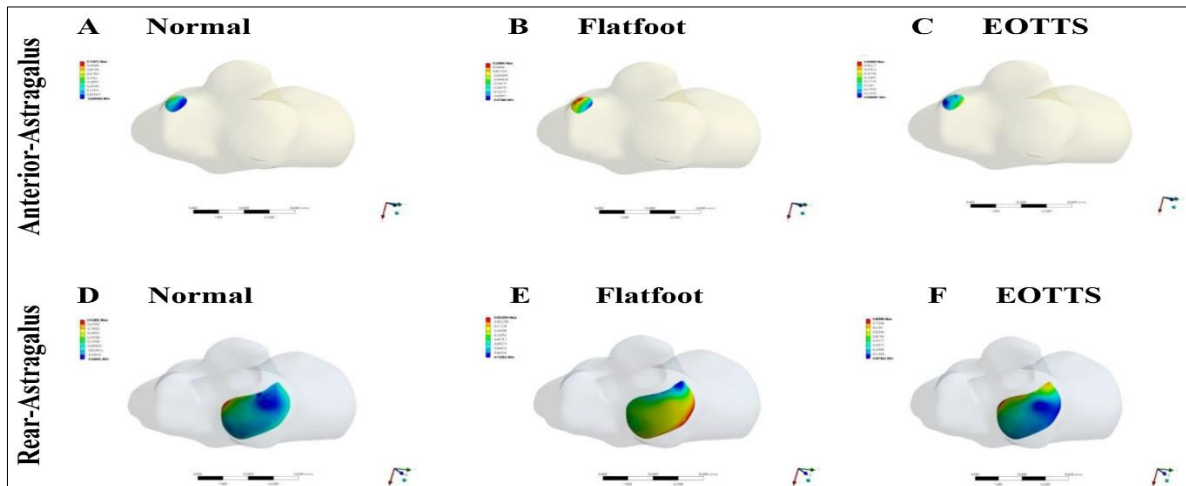| Paramet-ers	Astragalus joint surface				Calcaneal joint surface			
	Anterior-astragalus	Mid-astragalus	Rear-astragalus	Talona-vicular	Anterior-calcaneal	Mid-calcaneal	Rear-calcaneal	Calcane-ocuboid
Normal	55.4	107.8	380.6	356.6	56.3	117.5	394.2	233.9
Flatfoot	61.5	79.2	327.5	304.6	53.7	83.6	311.2	306.9
EOTTS	55.8	95.6	374.1	342.9	54.6	101.5	382.7	225.4

Figure 3: Cloud chart of maximum principal stress of each joint surface; top row are the (A) normal, (B) flatfoot, (C) EOTTS of anterior-astragalus; bottom row are the (D) normal, (E) flatfoot, and (F) EOTTS of rear-astragalus.
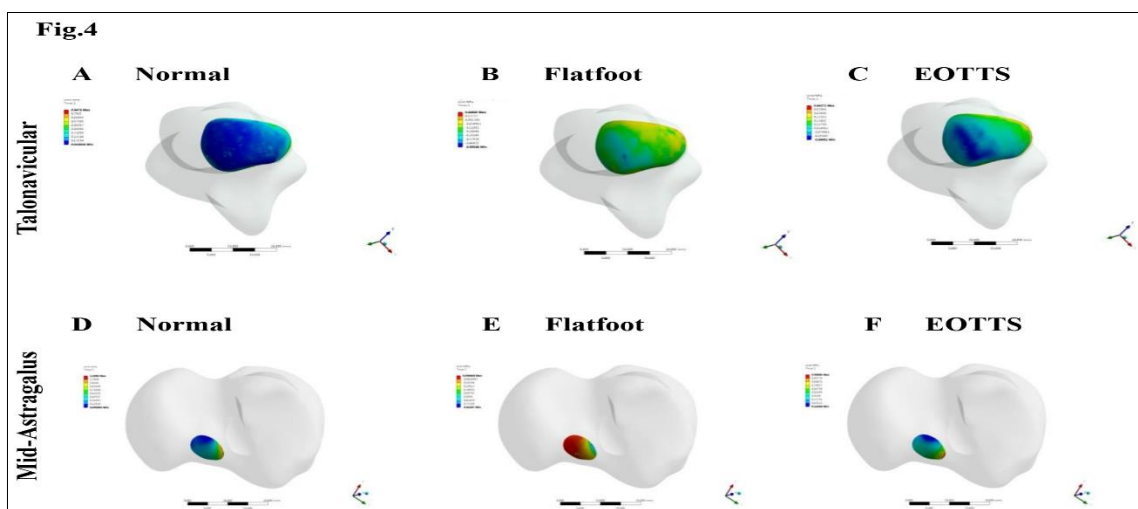

Figure 4: Cloud chart of the equivalent stress of von-Misesin each joint surface; top row are the (A) normal, (B) flatfoot, and (C) EOTTS of talonavicular; and bottom row are the (D) normal, (E) flatfoot, and (F) EOTTS of mid-astragalus.

Table 5: Coordinates of bones (mm).

Parameters	Astragalus			Calcaneus			Navicular			Cuboid		
	X-axis	Y-axis	Z-axis	X-axis	Y-axis	Z-axis	X-axis	Y-axis	Z-axis	X-axis	Y-axis	Z-axis
Normal	6.45	2.24	11.64	2.07	2.43	5.23	1.31	1.17	3.1	3.52	0.87	2.83
Flatfoot	3.75	2.81	8.23	7.88	2.84	2.24	2.07	1.12	4.6	7.23	0.98	4.2
EOTTS	6.32	2.45	10.87	2.8	2.62	4.75	1.42	1.16	3.63	4.19	0.92	2.68

DISCUSSION

The methods most commonly used to evaluate the effects of EOTTS are human motion analyses, follow-up investigations, and cadaveric experiments.[14,22,23] Gait analysis is the most frequently employed method used to examine human motion to assess surgical outcomes and rehabilitation.[23] FE analysis is effective for characterizing postoperative biomechanical changes and provides direct guidelines when assessing surgical options.[24] In 1972, Brekelmans et al introduced FE analysis into the medical field as a first group.[25] Now FE analysis has become widely used in orthopedic biomechanics research to analyze changes in internal stress, strain on bones, joints, and implants, contact area, and stress distribution.[26] This method is a feasible alternative to other available experimental methods and generates realistic simulations of in vivo conditions.[27] Computational analysis renders insight into contact pressure, distribution of internal stress, and deformation of individual subjects under load despite the presence of complex geometries and material properties.[28-30] Therefore, FE analysis could be employed to inform surgical decisions when treating various injuries to the foot and ankle. Recently, FE analysis has become widely used for biomechanical assessments of the foot and ankle due to its sophisticated computation and unique ability to include load and material properties.[29]

Along these lines, the 3D FE method is useful for analyzing the biomechanical characteristics of the subtalar joint.[31] In the present study, we established a 3D FE model of a normal human talus and characterized the structures around it using CT image sequences, which allowed an accurate simulation of the talus and surrounding anatomical structures. All three models in the present study originated from one volunteer's CT images, which reduces individual differences in the flexible flatfoot. An ideal model of flexible flatfoot in children must include the essential characteristics since most cases of flexible flatfoot are similar to each other. There is a broad consensus that simulations from normal volunteers to establish models of pathology are more acceptable than models from the diseased foot itself.[18] Such models could help better understand the biomechanical behavior of the flexible flatfoot and its surgical treatment. We calculated and assessed the changes in contact stress on the subtalar joint before and after EOTTS using 3D FE modeling. The purpose of this study was to provide a theoretical basis for the clinical application of EOTTS for treating flexible flatfoot in children.

The major finding of this study was that flexible flatfoot is attributed to subtalar joint instability, and shows that the stresses are more concentrated, increased local stress, abnormal stress distribution and abnormal movement of subtalar joint. The talus was partially dislocated from the calcaneus in the posterior to medial aspect during loading. Furthermore, partial dislocation was also associated with loading at the foot and ankle, which should be clinically recognized. In ideal treatments of flexible flatfoot, implants should both stabilize the subtalar joint and facilitate physiologic relative motion; EOTTS may allow achievement of this goal.[32] Traditional surgeries require immobilization for a relatively long period, which can negatively impact functional recovery of the foot. Therefore, stent can mechanically stabilize the hindfoot and allow activity in the early stage.[33] There has been debate about device removal. Since the overall goal of treatment is to restore functioning of the joint, we propose the devices do not need to be removed until the bony structure reaches maturity.

Despite the valuable results obtained in the present study, there are some limitations inherent to modeling due to simplifications of several factors. First, it is difficult to determine typical values for mechanical characterization of materials when assessing human tissues. Second, experimental studies about the subtalar joint have been scarce and provide little data that can be used in our FE models.[34] Third, because many nonlinear problems are involved in modeling and calculation, the convergence of results can also be hard to control. This results in bones being considered homogeneous, isotropic, and linearly elastic. Articular cartilage deformation was overlooked due to bones being considered rigid and cartilage function was incorporated into the model by neglecting friction. These limitations, as well as others, such as simplification of stent geometry and model grid parameters, must be taken into account before directly translating these data into the clinic.[35]

Another limitation of this study was that the foot and ankle remained in a static standing position, despite foot and ankle motion being a dynamic process. Therefore, we will next study the dynamic flatfoot motion period. Individual differences in this study may have impacted the results. This study analyzed the effects of flexible flatfoot and EOTTS on subtalar joint stability based on interior stress changes, but other factors that affect the subtalar joint stability should be considered in practice. It is a relatively

simplified loading method with some differences between the model results and actual situation.

The etiology and biologic structure of flexible flatfeet in children are very complicated. Therefore, the 3D FE analysis of the effects of flexible flatfoot and EOTTS on subtalar biomechanics performed in this study was only preliminary. Overall, the findings of the present study will aid in clinical diagnoses and management of flexible flatfoot in children. The present FE analysis shows flexible flatfoot causes not only less contact area for the articular facet, but also abnormal stress distribution on the subtalar joint.

Therefore, a minimally invasive stabilization surgery is necessary when instability exists. EOTTS can effectively prevent excessive abnormal activity of the subtalar joint from flexible flatfoot, thus restoring physiologic biomechanical normality to the subtalar joint.

CONCLUSION

As the motion center of the hindfoot, subtalar articular surface dislocation can lead to flatfoot deformity and weight-bearing structural changes. These deformities result in biomechanical changes to the subtalar joint area, causing abnormal foot motion, ankle instability, and corresponding clinical symptoms. A 3D FE model of children's flexible flatfoot is both a correct and reliable model. It is a good method of studying the biomechanics of flexible flatfoot and EOTTS, an effective preoperative assessment tool, and can contribute to fully understanding the biomechanical properties of the subtalar joint in flexible flatfoot. EOTTS can restore the normal biomechanics of the subtalar joint and is effective for treating children's flexible flatfoot. With the development of FE technology and biomechanics, we can establish personalized models of flatfoot for patients and systematically analyze biomechanical changes in the entire foot in the future.

REFERENCES

1. Davitt JS, Beals TC, Bachus KN. The effects of medial and lateral displacement calcaneal osteotomies on ankle and subtalar joint pressure distribution. Foot Ankle Int. 2001;22(11):885-9.
2. Campbell ST, Reese KA, Ross SD, McGarry MH, Leba TB, Lee TQ. Effect of graft shape in lateral column lengthening on tarsal bone position and subtalar and talonavicular contact pressure in a cadaveric flatfoot model. Foot Ankle Int. 2014;35(11):1200-8.
3. Rockar PA. The subtalar joint: anatomy and joint motion. J Orthop Sports Phys Ther. 1995;21(6):361-72.
4. Graham ME, Parikh R, Goel V, Mhatre D, Matyas A. Stabilization of joint forces of the subtalar complex via HyProCure sinus tarsi stent. J Am Podiatr Med Assoc. 2011;101(5):390-9.
5. Wagner UA, Sangeorzan BJ, Harrington RM, Tencer AF. Contact characteristics of the subtalar joint: load distribution between the anterior and posterior facets. J Orthop Res. 1992;10(4):535-43.
6. Ronneberger O, Fischer P, Brox T. U-Net: Convolutional Networks for Biomedical Image Segmentation. In: Navab N, Hornegger J, Wells W, Frangi A, editors. Medical Image Computing and Computer-Assisted Intervention – MICCAI 2015. MICCAI 2015. Lecture Notes in Computer Science. Springer, Cham. 2015;9351.
7. Dare DM, Dodwell ER. Pediatric flatfoot: cause, epidemiology, assessment, and treatment. Curr Opin Pediatr. 2014;26(1):93-100.
8. Walters JL, Mendicino SS. The flexible adult flatfoot: anatomy and pathomechanics. Clin Podiatr Med Surg. 2014;31(3):329-36.
9. Graham ME, Jawrani NT, Chikka A, Rogers RJ. Surgical treatment of hyperpronation using an extraosseous talotarsal stabilization device: radiographic outcomes in 70 adult patients. J Foot Ankle Surg. 2012;51(5):548-55.
10. Kobayashi T, Saka M, Suzuki E,Yamazaki N, Suzukawa M, Akaike A, et al. In vivo kinematics of the talocrural and subtalar joints during weightbearing ankle rotation in chronic ankle instability. Foot Ankle Spec. 2014;7(1):13-9.
11. Bresnahan PJ, Chariton JT, Vedpathak A. Extraosseous talotarsal stabilization using HyProCure(R): preliminary clinical outcomes of a prospective case series. J Foot Ankle Surg. 2013;52(2):195-202.
12. Graham ME. Congenital talotarsal joint displacement and pes planovalgus: evaluation, conservative management, and surgical management. Clin Podiatr Med Surg. 2013;30(4):567-81.
13. Fernandez de Retana P, Alvarez F, Viladot R. Subtalar arthroereisis in pediatric flatfoot reconstruction. Foot Ankle Clin. 2010;15(2):323-35.
14. Graham ME, Jawrani NT, Goel VK. Effect of extra-osseous talotarsal stabilization on posterior tibial

nerve strain in hyperpronating feet: a cadaveric evaluation. J Foot Ankle Surg. 2011;50(6):672-5.

15. Nelson SC, Haycock DM, Little ER. Flexible flatfoot treatment with arthroereisis: radiographic improvement and child health survey analysis. J Foot Ankle Surg. 20014;43(3):144-55.

16. Badie F, Katouzian HR, Rostami M. A non-invasive measurement of the knee contact force using a subject-specific musculoskeletal model to investigate osteotomy. J Med Eng Technol. 2018;1-8.

17. Ruozi B, Belletti D, Manfredini G, Tonelli M, Sena P, Vandelli MA, et al. Biodegradable device applied in flatfoot surgery: comparative studies between clinical and technological aspects of removed screws. Mater Sci Eng C Mater Biol Appl. 2013;33(3):1773-82.

18. Camacho DL, Ledoux WR, Rohr ES, Sangeorzan BJ, Ching RP. A three-dimensional, anatomically detailed foot model: a foundation for a finite element simulation and means of quantifying foot-bone position. J Rehabil Res Dev. 2002;39(3):401-10.

19. Cheung JT, Zhang M, Leung AK, Fan YB. Three-dimensional finite element analysis of the foot during standing--a material sensitivity study. J Biomech. 2005;38(5):1045-54.

20. Guiotto A, Sawacha Z, Guarneri G, Avogaro A, Cobelli C. 3D finite element model of the diabetic neuropathic foot: a gait analysis driven approach. J Biomech. 2014;47(12):3064-71.

21. Wang Z, Imai K, Kido M, Ikoma K, Hirai S. A finite element model of flatfoot (Pes Planus) for improving surgical plan. Conf Proc IEEE Eng Med Biol Soc. 2014;844-7.

22. De Pellegrin M, Moharamzadeh D, Strobl WM, Biedermann R, Tschauner C, Wirth T. Subtalar extra-articular screw arthroereisis (SESA) for the treatment of flexible flatfoot in children. J Child Orthop. 2014;8(6):479-87.

23. Graham ME, Jawrani NT. Extraosseous talotarsal stabilization devices: a new classification system. J Foot Ankle Surg. 2012;51(5):613-9.

24. Yu JH, Wang YT, Lin CL. Customized surgical template fabrication under biomechanical consideration by integrating CBCT image, CAD system and finite element analysis. Dent Mater J. 2018;37(1):6-14.

25. Brekelmans WA, Poort HW, Slooff TJ. A new method to analyse the mechanical behaviour of skeletal parts. Acta Orthop Scand. 1972;43(5):301-17.

26. Fitzgerald RH, Vedpathak A. Plantar pressure distribution in a hyperpronated foot before and after intervention with an extraosseous talotarsal stabilization device-a retrospective study. J Foot Ankle Surg. 2013;52(4):432-43.

27. Christensen JC, Campbell N, DiNucci K. Closed kinetic chain tarsal mechanics of subtalar joint arthroereisis. J Am Podiatr Med Assoc. 1996;86(10):467-73.

28. Zanolli DH, Glisson RR, Nunley JA, Easley ME. Biomechanical assessment of flexible flatfoot correction: comparison of techniques in a cadaver model. J Bone Joint Surg Am. 2014;96(6)45.

29. Razak AH, Zayegh A, Begg RK, Wahab Y. Foot plantar pressure measurement system: a review. Sensors (Basel). 2012;12(7):9884-912.

30. Chockalingam N, Healy A, Naemi R, Burgess-Walker P, Abdul Razak AH, Zayegh A, et al. Comments and reply to: Foot plantar pressure measurement system: a review. Sensors (Basel). 2013;13(3):3527-8.

31. Chen WM, Park J, Park SB, Shim VP, Lee T. Role of gastrocnemius-soleus muscle in forefoot force transmission at heel rise - A 3D finite element analysis. J Biomech. 2012;45(10):1783-9.

32. Xu J, Zhang Y, Muhammad H, Wang X, Huang, J., Zhang, C., et al. (2015). In vivo three-dimensional analysis of hindfoot kinematics in stage II PTTD flatfoot. J Orthop Sci. 2015;20(3):488-97.

33. Shin, J., Yue, N., & Untaroiu, C. D. (2012). A finite element model of the foot and ankle for automotive impact applications. Ann Biomed Eng. 2012;40(12):2519-31.

34. Liu Q, Zhao G, Yu B, Ma J, Li Z, Zhang K. Effects of inferior tibiofibular syndesmosis injury and screw stabilization on motion of the ankle: a finite element study. Knee Surg Sports Traumatol Arthrosc. 2016;24(4):1228-35.

35. Yuan CS, Chen W, Chen C, Yang GH, Hu C, Tang KL. Effects on Subtalar Joint Stress Distribution After Cannulated Screw Insertion at Different Positions and Directions. J Foot Ankle Surg. 2015;54(5):920-6.